CORONAVIRUS

Protection of K18-hACE2 mice and ferrets against SARS-CoV-2 challenge by a single-dose mucosal immunization with a parainfluenza virus 5–based COVID-19 vaccine

Dong An[1†], Kun Li[2†], Dawne K. Rowe[1†], Maria Cristina Huertas Diaz[1], Emily F. Griffin[1], Ashley C. Beavis[1], Scott K. Johnson[3], Ian Padykula[1], Cheryl A. Jones[3], Kelsey Briggs[1], Geng Li[1], Yuan Lin[1], Jiachen Huang[1], Jarrod Mousa[1,3], Melinda Brindley[1], Kaori Sakamoto[4], David K. Meyerholz[5], Paul B. McCray Jr.[2,6]*, S. Mark Tompkins[1,3]*, Biao He[1]*

Transmission-blocking vaccines are urgently needed to reduce transmission of SARS-CoV 2, the cause of the COVID-19 pandemic. The upper respiratory tract is an initial site of SARS-CoV-2 infection and, for many individuals, remains the primary site of virus replication. An ideal COVID-19 vaccine should reduce upper respiratory tract virus replication and block transmission as well as protect against severe disease. Here, we optimized a vaccine candidate, parainfluenza virus 5 (PIV5) expressing the SARS-CoV-2 S protein (CVXGA1), and then demonstrated that a single-dose intranasal immunization with CVXGA1 protects against lethal infection of K18-hACE2 mice, a severe disease model. CVXGA1 immunization also prevented virus infection of ferrets and blocked contact transmission. This mucosal vaccine strategy inhibited SARS-CoV-2 replication in the upper respiratory tract, thus preventing disease progression to the lower respiratory tract. A PIV5-based mucosal vaccine provides a strategy to induce protective innate and cellular immune responses and reduce SARS-CoV-2 infection and transmission in populations.

INTRODUCTION

Severe acute respiratory syndrome coronavirus 2 (SARS-CoV-2) was first identified in Wuhan, China in December 2019 as a cause of pneumonia and has subsequently spread globally to cause the coronavirus disease 2019 (COVID-19) pandemic. The virus has infected more than 145 million people worldwide, caused more than 3,079,000 deaths as of 24 April 2021, and is poised to continue to spread in the absence of herd immunity (https://who.int/emergencies/diseases/novel-coronavirus-2019). Social distancing, use of personal protective equipment, and widespread testing with contact tracing, quarantine procedures, and limited supplies of vaccines under Emergency Use Authorization (EUA) are currently the only measures available to limit virus spread. A vaccine that prevents mortality and reduces transmission is urgently needed.

The sinonasal epithelium of the upper respiratory tract is an initial site of SARS-CoV-2 infection, and for many individuals, it remains the primary site of virus replication. High levels of viral replication occur in the upper respiratory tract (*1*), and nasopharyngeal shedding can continue for several days following initial presentation (*2*). Progressive lower respiratory tract manifestations of pneumonia, acute respiratory distress syndrome, and respiratory failure contribute to much of the COVID-19 morbidity and mortality, and there is increasing evidence of involvement of other organ systems beyond the lungs. Because the upper and lower respiratory tracts are critical sites of COVID-19 pathogenesis, stopping viral replication in the upper respiratory tract before progression to the lung is an important goal for a protective vaccine. Leading vaccines to date generated robust antibody responses in immunized animals and in human clinical trials and reduced SARS-CoV-2 replication in the lower respiratory tract in nonhuman primate models (*3*–*7*). However, complete protection in the upper respiratory tract, which is important to prevent SARS-CoV-2 transmission, has been difficult to achieve. There are currently no reports on whether these vaccine candidates can block transmission.

Parainfluenza virus type 5 (PIV5) is a negative-stranded RNA virus in the family Paramyxoviridae that has been evaluated as a vaccine vector for influenza, respiratory syncytial virus (RSV), rabies, and a variety of other pathogens (*8*–*12*). In animal models, PIV5 is safe and is not associated with any disease, with the exception of kennel cough in dogs (*13*). Intranasally administered kennel cough vaccines containing live PIV5 have been used for more than four decades with an excellent safety record. Dogs immunized with kennel cough vaccines can shed PIV5 for up to 5 days, and it has been safe to humans in close contact with immunized animals (*14*, *15*). PIV5 is particularly well suited as a vaccine vector for respiratory diseases, as when administered intranasally, it elicits locally protective immunoglobulin A (IgA) responses in the respiratory tract as well as systemic innate and adaptive immune responses (*16*). Recently, a single intranasal dose of a PIV5-based Middle East respiratory syndrome (MERS) vaccine induced neutralizing antibodies and cellular immune responses and was 100% protective against a lethal challenge with MERS-CoV in a murine model of MERS (*9*). The study provides proof of concept for PIV5 as a candidate for protection against SARS-CoV-2. In this work, we generated a recombinant PIV5 containing the full-length spike of SARS-CoV-2 with

[1]Department of Infectious Diseases, University of Georgia College of Veterinary Medicine, Athens, GA 30602, USA. [2]Department of Pediatrics, University of Iowa, Iowa City, IA 52242, USA. [3]Center for Vaccines and Immunology, University of Georgia College of Veterinary Medicine, Athens, GA 30602, USA. [4]Department of Pathology, University of Georgia College of Veterinary Medicine, Athens, GA 30602, USA. [5]Department of Pathology, University of Iowa, Iowa City, IA 52242, USA. [6]Department of Microbiology and Immunology, University of Iowa, Iowa City, IA 52242, USA.
*Corresponding author. Email: paul-mccray@uiowa.edu (P.B.M.); smt@uga.edu (S.M.T.); bhe@uga.edu (B.H.)
†These authors contributed equally to this work.

its cytoplasmic tail replaced with that of PIV5 F protein (CVXGA1) and tested its efficacy as a vaccine in mice and ferrets.

RESULTS

Generation and analysis of PIV5 expressing the S protein of SARS-CoV-2 (CVXGA1)

Using a strategy similar to that used in PIV5-based MERS-CoV vaccine development, we generated a PIV5 expressing the SARS-CoV-2 Spike (S) protein (termed CVXGA1) (Fig. 1A). We not only confirmed the viral genome sequence by reverse transcription polymerase chain reaction (RT-PCR) sequencing but also confirmed expression of the S glycoprotein in CVXGA1-infected cells using immunofluorescence and Western blot (Fig. 1B). Besides full-length S, a cleaved product, S1, was also detected in CVXGA1-infected cells, indicating that S was processed (Fig. 1B). The S protein mediates cell-to-cell fusion and virus-to-cell fusion to facilitate viral entry, and immunization with S generates protective immunity against SARS-CoV-2 (*6*). It is thought that the native (containing prefusion) conformation of S induces desirable immunity for optimal protection (*6*). To examine whether the S protein expressed by the PIV5 vector is functional, Vero cells, which express the angiotensin-converting enzyme 2 (ACE2)

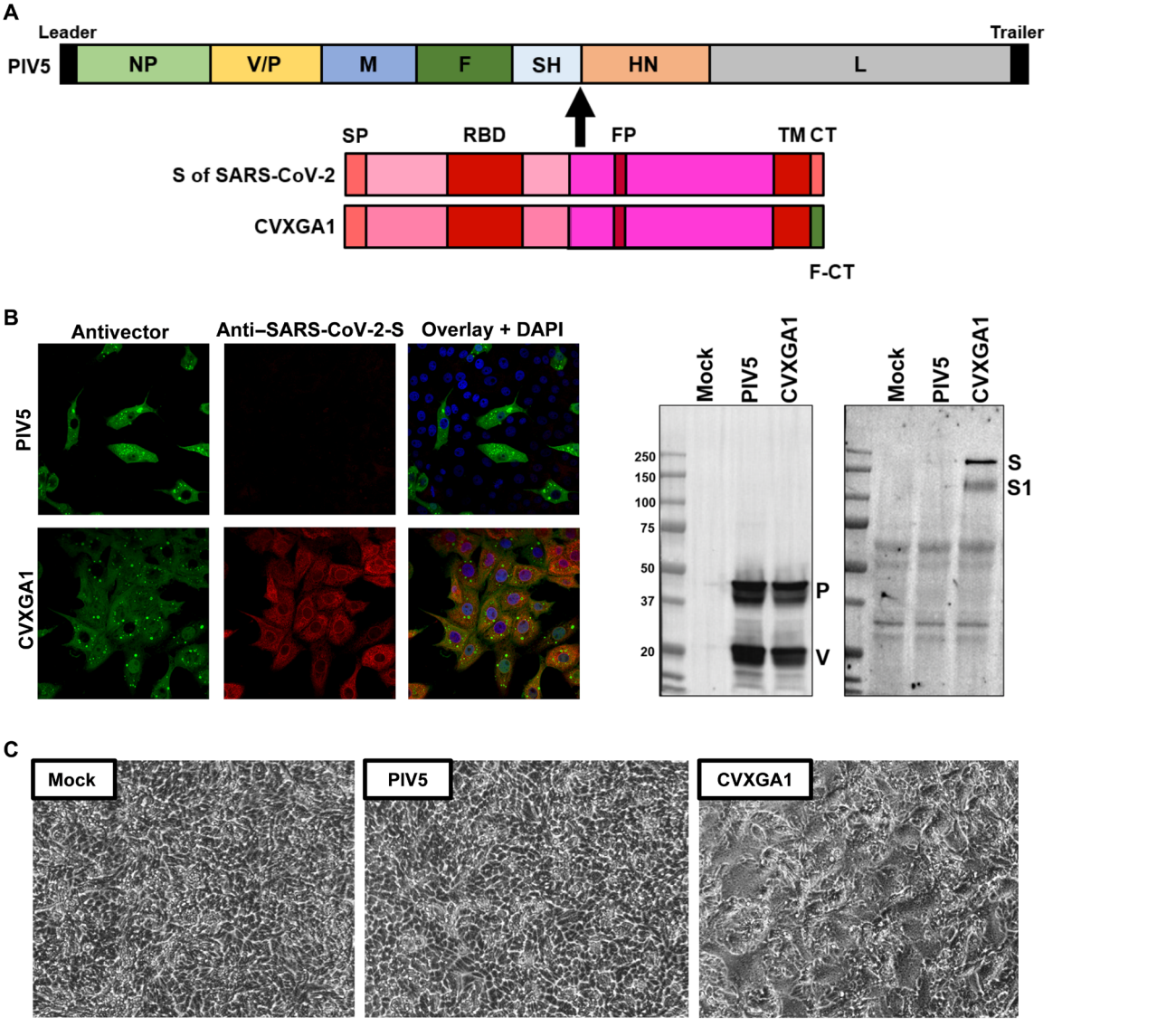

Fig. 1. Generation of CVXGA1 and analysis of CVXGA1 in tissue culture cells. (**A**) Schematic of CVXGA1. PIV5 has seven genes and encodes eight proteins, NP, V, P, M, F, SH, HN, and L. Leader and trailer sequences are important for viral RNA synthesis. S of SARS-CoV-2 contains signal peptide (SP), RBD, fusion peptide (FP), transmembrane domain (TM), and cytoplasmic tail (CT). In CVXGA1, the CT of S was replaced with F and inserted between the PIV5 SH and HN coding sequences. (**B**) Detection of S expression. To detect SARS-CoV-2-S expression, immunofluorescence assays were performed. MDBK cells were mock-infected or infected at 1 MOI with PIV5 or CVXGA1. Two days post-infection, the cells were fixed, permeabilized, and stained with DAPI, along with antibodies specific for PIV5-V/P (antivector, green) and SARS-CoV-2 S (red). To detect expression using immunoblotting, Vero cells were infected with PIV5 and CVXGA1 at 1 MOI and lysed at 24 hpi. The lysates were resolved on an SDS-PAGE gel and immunoblotted with anti-SARS-CoV-2 S and anti–PIV5-V/P. (**C**) Syncytia formation caused by CVXGA1. Vero cells were infected with PIV5 or CVXGA1 at an MOI of 0.1. At 48 hours after infection, photomicrographs of the cells were obtained.

receptor, were infected with CVXGA1. Syncytia formation (cell-to-cell fusion) was observed only in CVXGA1-infected cells, indicating functional expression of the S protein (Fig. 1C).

CVXGA1 generated humoral and cellular immune responses in mice

To investigate CVXGA1 antigenicity, we first immunized mice intranasally with a range of CVXGA1 inocula. A dose-dependent increase in anti-S antibodies was detected in BALB/c mice after a single intranasal administration (Fig. 2A). Similarly, antibodies recognizing the receptor binding domain (RBD) of S were detected in a dose-dependent manner in BALB/c mice immunized with CVXGA1 (Fig. 2B). Furthermore, neutralizing antibodies against SARS-CoV-2 were detected in BALB/c mice immunized in a dose-dependent manner (Fig. 2C). Substantial antibody generation and cellular responses were observed in C57BL/6 mice after a single intranasal immunization with a dose as low as 6×10^3 plaque-forming units (PFU) of CVXGA1 (fig. S1). These results indicate that a single intranasal dose immunization with CVXGA1 generated robust immune responses in mice.

CVXGA1 protected mice with human ACE2 receptor against SARS-CoV-2 lethal challenge

To determine CVXGA1 efficacy, we used two complementary animal models: a severe disease model using transgenic mice and an upper respiratory tract infection model using ferrets. Mice lack a functional ACE2 receptor for SARS-CoV-2 and thus are resistant to infection. To examine vaccine efficacy in a very stringent model, we used human ACE2 (hACE2) transgenic mice. Mice expressing hACE2 under regulation of the cytokeratin 18 promoter (K18), originally developed to study SARS-CoV infection (*17*), were recently demonstrated to develop severe lung disease in response to SARS-CoV-2 infection (*18*, *19*). Inoculation of K18-hACE2 mice with 10^5 PFU of SARS-CoV-2 results in 100% mortality, lung disease with signs of diffuse alveolar damage, and variable spread to the central nervous system. The lethal dose, 50% (LD_{50}), is estimated to be 10^4 PFU (*18*, *19*). K18-hACE2 mice were immunized intranasally with a single dose of CVXGA1 (10^6 PFU) and, 4 weeks later, challenged with 4×10^4 PFU of SARS-CoV-2. Another group of K18-ACE2 mice was immunized intramuscularly with ultraviolet (UV)–inactivated SARS-CoV-2 and then boosted 2 weeks later. Nonvaccinated mice received intramuscular Dulbecco's modified Eagle's medium (DMEM). A second control group was immunized intranasally with a single dose of PIV5 vector intranasally (10^6 PFU). In response to the SARS-CoV-2 challenge, the DMEM control group lost weight and succumbed to infection by 7 days post-challenge (dpc) (Fig. 3, A and B). Mice immunized with UV-inactivated SARS-CoV-2 or PIV5 lost as much weight as the DMEM group. All PIV5-immunized mice succumbed by 7 dpc, and four of six UV-inactivated SARS-CoV-2–immunized mice died (Fig. 3, A and B). CVXGA1-immunized mice lost no weight and all survived (Fig. 3, A and B).

At 5 dpc, virus titers in the lung tissue of mice immunized with DMEM, UV-inactivated SARS-CoV-2, or PIV5 were similar (Fig. 3C), and all three groups demonstrated evidence of brain infection (Fig. 3D). In contrast, CVXGA1-immunized mice had no detectable SARS-CoV-2 in lung tissue, demonstrating a ~5 log reduction in virus titer (Fig. 3C). Notably, four of four CVXGA1-immunized mice had no virus detected in brain tissue (Fig. 3D) after SARS-CoV-2 challenge.

Five days after SARS-CoV-2 challenge, we localized virus antigen (N protein) in lung tissues. Control DMEM-treated animals had diffuse antigen staining throughout the airway and lung parenchymal epithelial cells (Fig. 4A). In contrast, CVXGA1-immunized mice exhibited only uncommon small foci of N protein–positive cells, presumptively indicative of initial infection sites that did not progress (Fig. 4A). Lung tissues from UV-inactivated SARS-CoV-2 and PIV5 treatment groups both showed diffuse antigen-positive cells (Fig. 4A).

Lung tissue sections from animals infected with SARS-CoV-2 were examined and scored for the presence of perivascular eosinophilic infiltrates. At 5 days after infection, an influx of eosinophils was clearly evident in the mice immunized with UV-inactivated SARS-CoV-2 and absent from the other groups (Fig. 4B, inset arrows). Lung tissues were also scored for the presence of perivascular inflammatory cell infiltrates. Perivascular pulmonary infiltrates, when comprised mostly of lymphoid cells, can be a favorable sign of previous antigenic exposure and effective vaccination. As shown in Fig. 4B, compared to the DMEM control group, CVXGA1-immunized

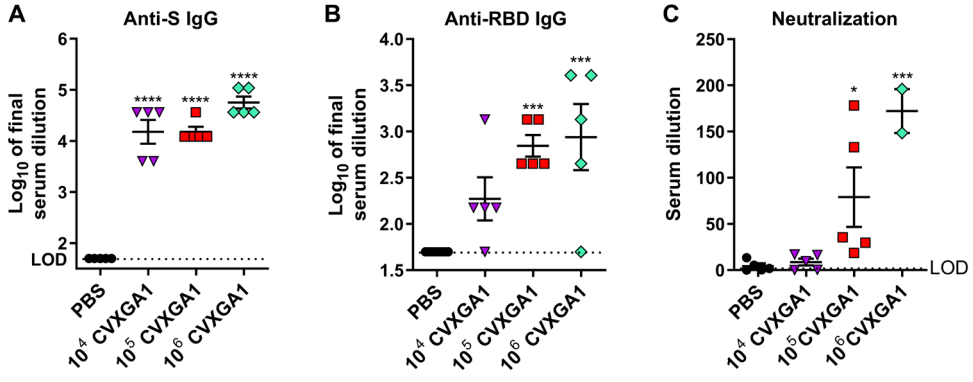

Fig. 2. Immunogenicity of CVXGA1 in mice. (**A**) Anti-S titers in BALB/c mice immunized with CVXGA1. BALB/c mice ($n = 5$ per group) were immunized via intranasal route with CVXGA1 at a dose of 10^4, 10^5, and 10^6 PFU. At 28 dpi, mice were bled, and anti-S titers were measured using ELISA. Error bars represent the SEM, and *P* values were calculated with one-way analysis of variance (ANOVA). ****$P < 0.0001$. (**B**) Anti-RBD titers in BALB/c mice immunized with CVXGA1. Titers of RBD of samples in (**D**) were determined using ELISA. Error bars represent the SEM, and *P* values were calculated with one-way ANOVA. ***$P < 0.001$. (**C**) Neutralization titers in BALB/c mice immunized with CVXGA1. Neutralization titers were determined as described in Materials and Methods. Error bars represent the SEM, and *P* values were calculated with one-way ANOVA. *$P < 0.05$ and ***$P < 0.001$. LOD, limit of detection.

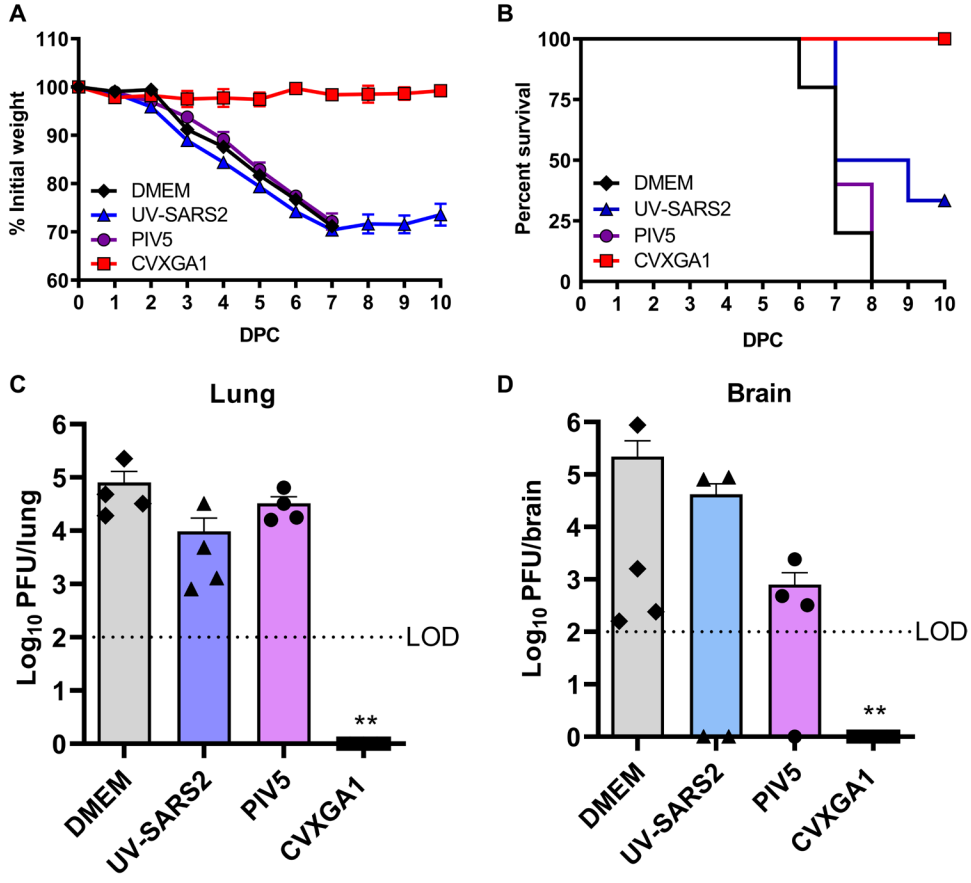

Fig. 3. Intranasal vaccination with CVXGA1 protects K18-hACE2 transgenic mice against SARS-CoV-2 infection. Mice received DMEM intranasally, CVXGA1 immunization via intranasal (10^6 PFU) route, UV-inactivated SARS-CoV-2 (UV-SARS2) administered via intramuscular route with alum adjuvant followed by a boost dose at 21 dpi, and wild-type PIV5 (10^6 PFU) via intranasal route. Five weeks following immunization, K18-hACE2 mice were intranasally infected with 4×10^4 PFU of SARS-CoV-2 in 50 μl of DMEM. Error bars represent the SEM. (**A**) Weight loss and (**B**) survival outcomes in K18-hACE2 transgenic mice. Weight changes in 6- to 8-week-old mice were monitored daily (DMEM, $n = 9$; CVXGA1, $n = 8$; UV-inactivated SARS-CoV-2, $n = 10$ mice per group; PIV5, $n = 10$). CVXGA1-immunized mice lost no weight and survived. All DMEM- and PIV5-treated mice succumbed. One UV-inactivated SARS-CoV-2–treated mouse survived. Days after infection with SARS-CoV-2 denoted by dpi (**C** and **D**) CVXGA1 vaccine reduces lung tissue titer and prevents viral spread to the brain. Five days after SARS-CoV-2 infection, lung ($n = 4$) and brain ($n = 4$) tissues were obtained from groups in (A) and (B) and titrated. See Materials and Methods for details. Error bars represent the SEM. $^{**}P < 0.01$; one-way ANOVA with Dunnett's posttest.

mice had a significant increase in perivascular lymphoid cell infiltrates.

The presence of interstitial disease is often a hallmark of severe viral pneumonia. Lung tissues were examined and scored for the presence of interstitial disease (H score), defined by the presence of alveolar septal infiltration, extension into the airspaces, and associated atelectasis and edema. Compared to the other treatment groups, CVXGA1-immunized mice had the least evidence of interstitial disease at 5 days after SARS-CoV-2 challenge (Fig. 4C). Histopathologic scores for eosinophilic infiltrates, perivascular infiltrates, and severity of interstitial lung disease are presented in Fig. 4D. Furthermore, we examined the efficacy of CVXGA1 immunization against a high challenge dose (10^6 PFU of SARS-CoV-2 per mouse) and found that CVXGA1 immunization protected 100% of mice from this lethal challenge (fig. S2).

CVXGA1 protected ferrets from SARS-CoV-2 infection

Ferrets are a widely used model of human respiratory infections, are susceptible to SARS-CoV-2 infection, and can transmit the virus to other animals via direct contact and aerosol (*20*–*22*). To test CVXGA1 efficacy in ferrets, animals were immunized intranasally with phosphate-buffered saline (PBS) or CVXGA1 (Fig. 5A). CVXGA1 replicated in the nasal cavities of ferrets at 3 and 7 days post-immunization (dpi) with a peak titer greater than 10^4 PFU/ml in nasal washes, and CVXGA1 was cleared by 14 dpi (fig. S3A). CVXGA1 immunization generated robust antibody responses as evidenced by high titers of anti-S IgG (fig. S3B), anti-RBD IgG (Fig. 5B), and neutralizing antibodies in Fig. 5C. Low levels of anti-S IgA were detected in nasal washes (fig. S3C). When challenged with SARS-CoV-2 intranasally, no viral genome RNA was detected in nasal washes from CVXGA1-immunized ferrets (Fig. 6A). In contrast, viral RNA was detected in all mock-immunized ferrets over time (Fig. 6A). Viral RNA was also detected in the trachea and lungs of mock-immunized ferrets but not in the trachea and lungs of CVXGA1-immunized ferrets (Fig. 6, B and C). To assess SARS-CoV-2 exposure in ferrets, anti-S antibody levels were quantified at the time of experiment termination (7 dpc). Anti-S IgG levels in the CVXGA1-immunized group increased after challenge (fig. S3D), indicative of a memory response and exposure to the S antigen. These results indicate that CVXGA1 immunization markedly reduced SARS-CoV-2

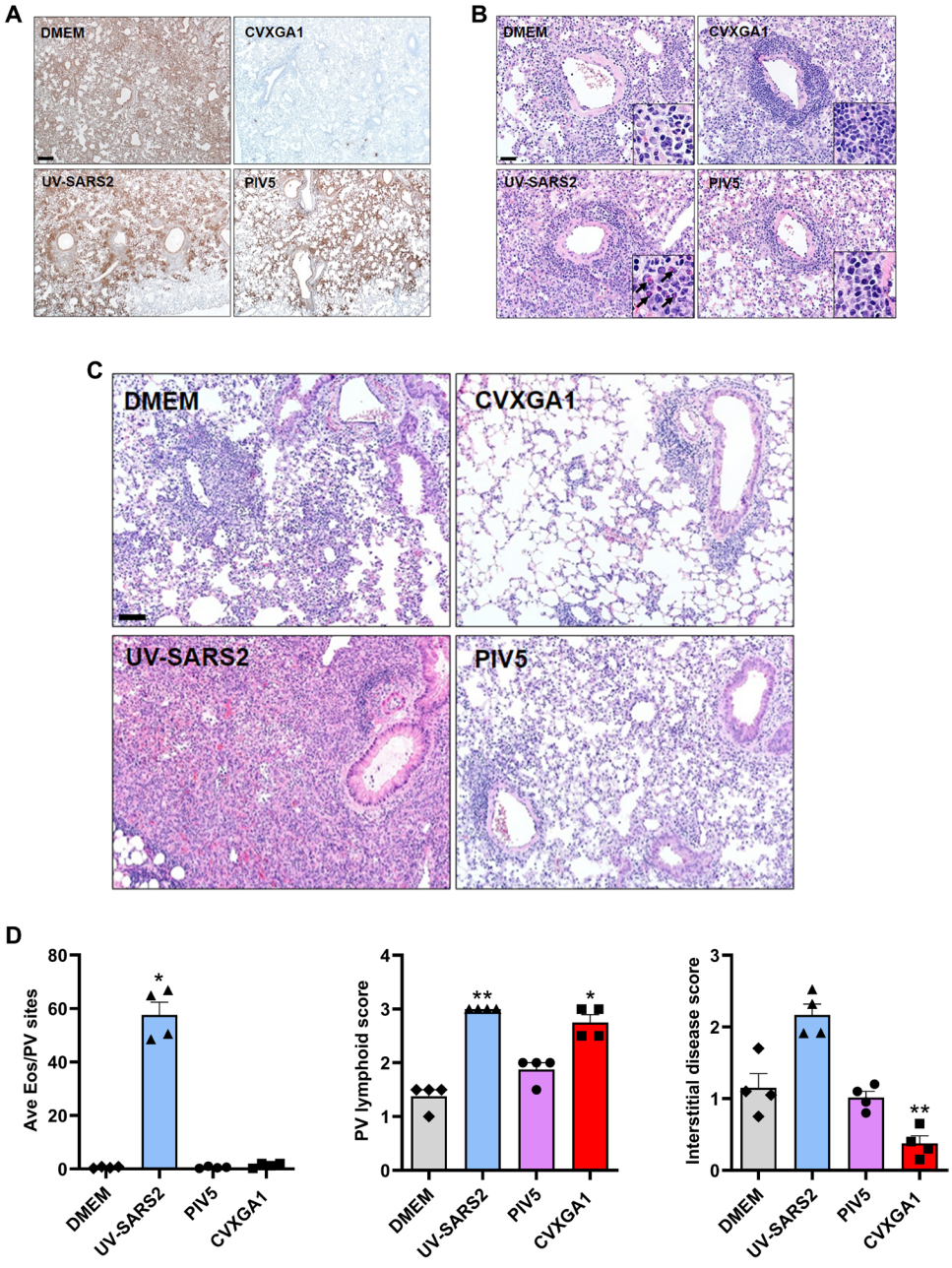

Fig. 4. Histopathologic analysis of SARS-CoV-2 infection in K18-hACE2 transgenic mice immunized with CVXGA1. (**A** to **C**) Histology of fixed lung tissues, 5 days after SARS-CoV-2 infection. Representative images of SARS-CoV-2–infected mice that received DMEM, CVXGA1, UV-SARS2, or PIV5. (A) Representative distribution of virus antigen (N protein, brown stain) in lung tissues from indicated groups ($n = 4$ per group). Note the rare focal immunostaining in CVXGA1 group compared to diffuse immunostaining in other groups. Scale bar, 220 μm. (B) H&E-stained tissues ($n = 4$ per group). Eosinophilic infiltrates were only noted in the UV-SARS2 group (arrows in inset; scale bar, 45 μm). (C) H&E-stained tissues ($n = 4$ per group). Interstitial lung disease was reduced in the CVXGA1. Scale bar, 90 μm. (**D**) Histopathologic scoring of lung tissues (see Materials and Methods for details; $n = 4$ per group). Tissues from all four groups were ordinally scored for eosinophilic infiltrates, perivascular infiltrates, and interstitial lung disease. Error bars represent the SEM. $^*P < 0.05$ and $^{**}P < 0.01$, one-way ANOVA with Dunnett's posttest.

replication in the upper respiratory tract, a site critical for SARS-CoV-2 onset.

To determine whether CVXGA1 immunization can block transmission, ferrets were immunized with a single dose of CVXGA1 as before. Control animals were immunized with PBS or empty PIV5 virus vector (Fig. 7A). Forty-two days after intranasal immunization, ferrets were challenged with SARS-CoV-2, and nasal washes were collected at 1, 3, 5, 7, 9, and 11 dpc (Fig. 7A). Naïve ferrets were cohoused with the challenged ferrets at a ratio of 1 naïve:1 infected beginning at 2 dpc (2 ferrets per cage). Because of animal welfare regulations, all ferrets were housed in open cages in the Biosafety Level 3 (BSL3) facility (fig. S4). All ferrets in the PBS and empty PIV5 vector groups became infected as indicated by detection of live SARS-CoV-2 in nasal secretions, peaking at 3 dpc (Fig. 7B). All

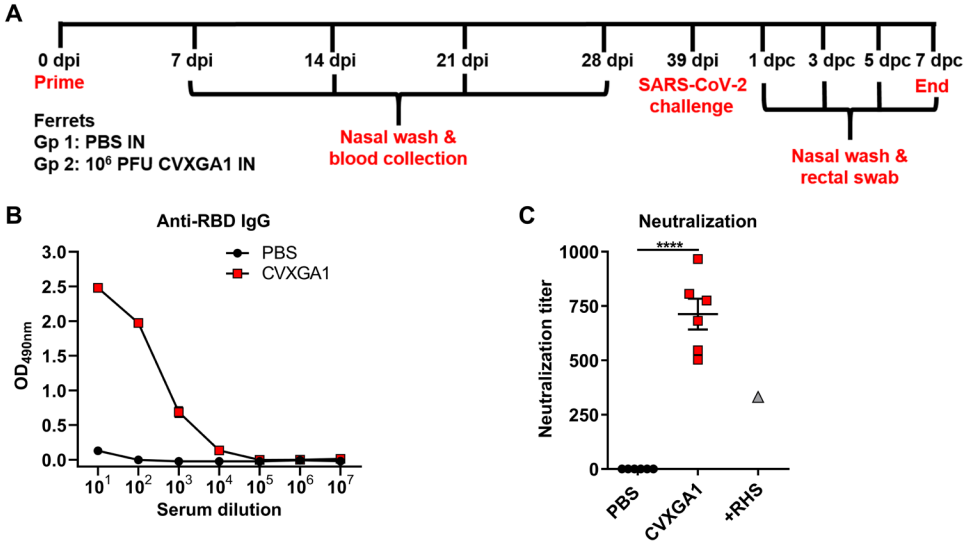

Fig. 5. Immunogenicity of CVXGA1 in ferrets. (**A**) Schematic of ferret immunization and viral challenge. Groups of six ferrets were immunized (CVXGA1) or mock-immunized (PBS) at a dose of 10^6 PFU intranasally (IN). Ferrets were challenged at 39 dpi with 4×10^5 PFU of SARS-CoV-2 intranasally. Nasal washes and rectal swabs were performed at 1, 3, 5, and 7 dpc. Half ($n = 6$) of the ferrets were humanely euthanized 4 days after challenge. The study ended at 7 dpc. (**B**) Anti-RBD serum IgG in ferrets after immunization. Serum anti-RBD IgG titers were evaluated via ELISA. Titers of 28 dpi are shown. Error bars represent the SEM. (**C**) Neutralization titers after immunization. Anti–SARS-CoV-2 neutralization titers at 28 dpi were determined using a VSV-CoV-SARS2-S virus. The +RHS (positive recovered human serum) was used as a positive control, and media alone was used as a negative control. Error bars represent the SEM, and *P* values were calculated with one-way ANOVA. ****$P < 0.0001$.

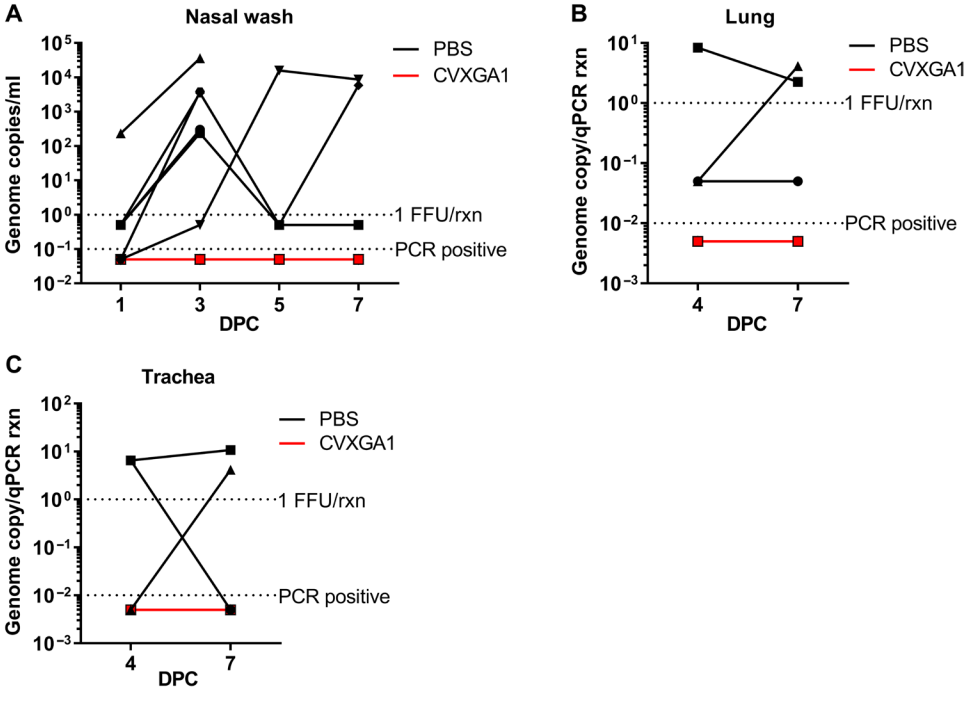

Fig. 6. Efficacy of CVXGA1 in ferrets. (**A**) Detection of viral RNA in 1, 3, 5, and 7 dpc nasal wash via qRT-PCR. Viral RNA was quantified as genome copies per milliliter and presented as $\log_{10}$ genome per milliliter as described in Materials and Methods. Each symbol represents a different animal (six PBS and six CVXGA1). PBS animals are black symbols, and CVXGA1-vaccinated animals are red symbols. One PFU/PCR reaction (rxn) is marked to differentiate between infectious viral particles and uninfectious genomic remnants. The limit of detection is indicated by the lowest dashed line. (**B**) Detection of viral RNA in lung tissues collected at 4 and 7 dpc via qRT-PCR. Viral RNA was quantified and presented as genome copies per reaction (rxn). (**C**) Detection of viral RNA in trachea tissues collected at 4 and 7 dpc via qRT-PCR. Viral RNA was quantified and presented as genome copies per reaction (rxn).

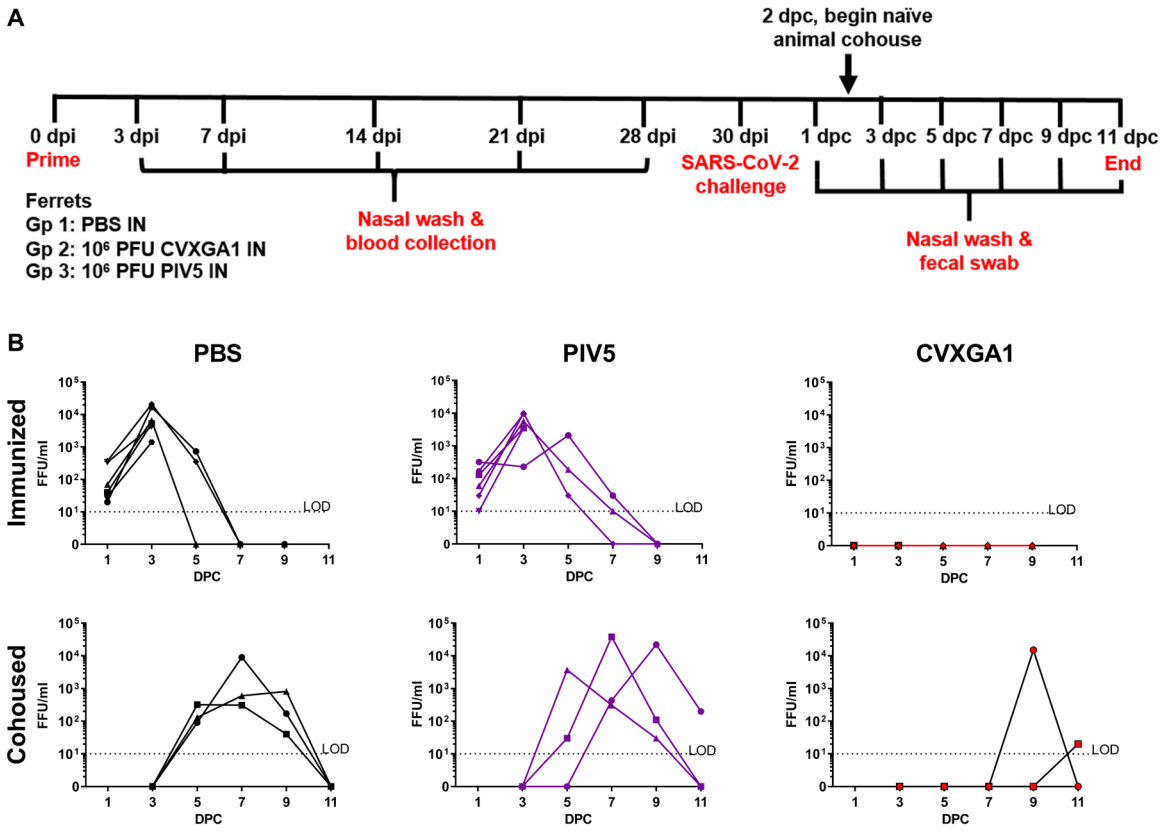

Fig. 7. Efficacy of transmission block by CVXGA1 immunization in ferrets. (**A**) Schematic of ferret immunization, viral challenge, and transmission. Groups of six ferrets were immunized (CVXGA1), with empty viral vector or mock-immunized (PBS) at a dose of 10^6 PFU intranasally. Ferrets were challenged at 42 dpi with 4×10^5 PFU of SARS-CoV-2 intranasally. Nasal washes were collected at 1, 3, 5, 7, 9, and 11 dpc. Half of the ferrets were humanely euthanized 4 days after challenge. The study ended at 11 dpc. At 2 dpc, one challenged ferret was mixed with one naïve ferret, and nasal washes were collected from naïve ferrets at 1, 3, 5, 7, and 9 days after mixing (3, 5, 7, 9, and 11 dpc, respectively). (**B**) Detection of SARS-CoV-2 at 1, 3, 5, 7, 9, and 11 dpc in nasal washes. Live virus was detected using FFA (FFU per milliliter) as described in Materials and Methods. Each symbol represents a different animal. The limit of detection is indicated by the lowest dashed line.

naïve ferrets cohoused with the infected PBS and empty PIV5 vector groups contracted SARS-CoV-2, with peak titers detected around 5 days after cohousing. The titers in the exposed naïve animals reached similar levels as those of directly infected animals, consistent with 100% transmission (Fig. 7B). As before (Fig. 5B), no virus was detected in nasal cavities of CVXGA1-immunized ferrets after challenge. No virus was detected in the naïve ferrets cohoused with CVXGA1-immunized and SARS-CoV-2–challenged ferrets for the first 5 days after cohousing (Fig. 7B), suggesting that direct contact with CVXGA1-immunized and challenged ferrets did not result in transmission of SARS-CoV-2 to naïve ferrets. Beginning 7 days after mixing, ferrets mixed with CVXGA1-immunized animals acquired infection, likely from the environment which included infected ferrets in neighboring cages (fig. S4).

DISCUSSION

This work demonstrates that a PIV5-based mucosal COVID-19 vaccine can prevent lethal disease in a mouse model and markedly reduce upper respiratory tract virus replication and inhibit transmission in ferrets. While no animal model completely reproduces all features of severe SARS-CoV-2 infection in humans, K18-hACE2 mice support robust virus replication and develop dose-dependent severe disease, but to date, transmission has not been studied in this model (*18*, *19*). In K18-hACE2 mice, the LD_{50} value is estimated to be 10^4 PFU (*19*, *23*). Prime boost of K18-hACE2 mice with UV-inactivated SARS-CoV-2 failed to protect 100% of mice from a lethal challenge. We note that when we used an estimated 100 LD_{50} challenge (10^6 PFU), mice immunized with inactivated virus lost more weight than the PBS control group (fig. S2). Similar to previous observations with a UV-inactivated MERS-CoV vaccine, immunization with UV-inactivated SARS-CoV-2 followed with 10^6 PFU of SARS-CoV-2 challenge triggered an influx of eosinophils, consistent with a hypersensitivity-type response (fig. S2E). K18-hACE2 mice that received sublethal SARS-CoV-2 inocula survived subsequent lethal dose challenge, but virus was detected in the lung tissue of surviving mice at 5 dpc (*18*). All mice immunized with a single dose of CVXGA1 survived an estimated 100 LD_{50} challenge (10^6 PFU) with no detectable virus in the brain, and 75% of the mice had no virus detected in lung tissue at 5 dpc, demonstrating the potent protective efficacy of CVXGA1.

Generating a native configuration of the viral glycoprotein as an antigen is desirable to maximize protective immune responses and may be challenging. Virus inactivation often results in undesirable changes in antigen conformation. To obtain optimal structure of purified viral glycoproteins, mutations are often introduced (*24*).

Previously, we demonstrated that PIV5 is an excellent vector to display the RSV F protein. Cells expressing F after infection with recombinant PIV5 containing F retain the same conformation as the native F protein in RSV-infected cells (*16*), demonstrating that a PIV5 live virus vector can appropriately express native viral glycoproteins. Expression of full-length SARS-CoV-2 S protein in CVXGA1-infected cells caused syncytia formation (Fig. 1C), consistent with display of a native, fusion-competent S protein. PIV5 enters host cells via F- and hemagglutinin and neuraminidase (HN)–mediated membrane fusion: HN binds to sialic acid residues on cell surface proteins, and F promotes membrane fusion. Since sialic acid residues are ubiquitous, PIV5 is known to infect practically all mammalian cells. Thus, expressing a functional S of SARS-CoV-2 does not expand cell tropism of CVXGA1 since CVXGA1 expresses S as well as F and HN (Fig. 1A). Furthermore, the accelerated syncytia formation promoted by CVXGA1 (PIV5 also causes syncytia in Vero E6 cells, albeit at a slower rate) is unlikely to cause damage as syncytia are more commonly observed in cells grown in monolayer culture and rarely occur in primary epithelial cells that are typically well differentiated and polarized.

Ferrets are very susceptible to SARS-CoV-2 infection and readily transmit the virus by direct contact and aerosol (*20*–*22*). Direct contact is a more efficient means of transmission than an indirect (aerosol) route. In published work, one infected ferret was cohoused with one or two naïve animals to study direct contact transmission (*20*, *22*). To test our vaccine in a robust transmission model, we cohoused one naïve ferret with one infected ferret (Fig. 7A and fig. S4). A single-dose intranasal CVXGA1 immunization completely protected against SARS-CoV-2 infection: No viral RNA was detected in nasal cavities of immunized animals (Fig. 6A). A single-dose CVXGA1 immunization inhibited direct transmission of SARS-CoV-2 (Fig. 7). Because the ferrets were housed in open cages, animals cohoused with CVXGA1-immunized ferrets became infected at 7 and 9 days after mixing, likely through environmental transmission from other cages. It is also possible that the late infections of naïve ferrets cohoused with CVXGA1-immunzed ferrets were a result of transmission by CVXGA1-immunized and SARS-CoV-2–challenged ferrets; thus, CVXGA1 just delayed transmission of SARS-CoV-2. However, no virus was detected in nasal washes or lungs of CVXGA1-immunized ferrets (fig. S5), suggesting that the likely source of virus for the cohoused ferrets was from infected ferrets housed in neighboring open cages. The lack of viral RNA in CVXGA1-immunzed ferrets after challenge supports that the late infection of ferrets cohoused with CVXGA1-immunized ferrets came from other infected ferrets (fig. S5). There were two possible routes by which naïve ferrets cohoused with CVXGA1-immunized/SARS-CoV-2–challenged ferrets became infected at later time points. One is that the ferrets acquired infection via aerosol transmission from infected ferrets in neighboring cages, as they were housed in open cages (fig. S4). Another possibility was contamination from husbandry and equipment: The procedure mandated by our IACUC (Institutional Animal Care and Use Committees) requires cage changes for the animals every 7 days. It is possible that the cohoused ferrets acquired infection through direct contact with contaminated equipment during these cage changes. We observed a disconnect between the viral RNA level and live virus in the PBS group (Fig. 7B and fig. S5): Live virus titers peaked at day 3 and were undetectable at day 7, while viral RNA first peaked at day 3 and had a high level at day 7. This delayed clearance of viral RNA may reflect methodologic differences, in which qRT-PCR can detect residual viral RNA. Intranasal CVXGA1 immunization generated robust serum antibody responses in mice and ferrets. Intranasal CVXGA1 immunization induced respiratory mucosal IgA in ferrets, consistent with previous report that PIV5 is a potent vector for vaccine development for respiratory infections, including influenza virus and RSV (*16*, *25*). Mucosal IgA was also detected in monkeys immunized intranasally with PIV5 expressing RSV F (*16*). As a live viral vector, we expect CVXGA1 to generate robust cellular immune responses, and as observed in fig. S1, cellular immune responses were detected in mice. Kennel cough vaccines have been produced inexpensively and safely used for many decades, and the manufacturing capacity and vaccine delivery systems for PIV5 are well established. Further development of a PIV5 vector–based vaccine may help block SARS-CoV-2 transmission and control the COVID-19 pandemic.

MATERIALS AND METHODS

Virus and cells

The CVXGA1 plasmid, encoding the full-length genome of PIV5 and a SARS-CoV-2 S protein gene with a cytoplasmic tail replaced with that of F of PIV5 and inserted between the PIV5 SH and HN genes, was constructed as previously reported (*26*). Virus rescue was performed as described previously (*26*). Briefly, the CVXGA1 plasmid and four helper plasmids—pPIV5-NP, pPIV5-P, pPIV5-L, and pT7-polymerase, encoding the NP, P, and L proteins and T7 RNA polymerase, respectively—were cotransfected into BHK21 cells at 90% confluence in 6-cm plates using Lipofectamine 3000 (Invitrogen). Virus released into the media was amplified in Vero cells. Recovery of virus is indicated by syncytia formation in Vero cells. The virus was then plaque-purified as a single plaque from Vero cells. The full-length genomes of the plaque-purified single clone of CVXGA1 virus were sequenced as described before (*26*). Viruses were grown in Vero cells for 5 to 7 days using DMEM containing 2% fetal bovine serum (FBS). Media were collected and pelleted at 3000 rpm to remove cell debris by using a Sorvall tabletop centrifuge for 10 min. Virus supernatant was supplemented with 10% sucrose-phosphate-glutamate buffer, snap-frozen in liquid nitrogen, and stored at −80°C immediately after collection.

SARS-CoV-2 virus (isolate USA-WA1/2020, BEI Resources, NR-52281) was propagated in Vero E6 cells cultured in DMEM + FBS at 37°C in 5% CO_2. Virus stocks or tissue homogenate supernatants were serially diluted in DMEM, inoculated on 12-well plates of Vero E6 cells at 37°C in 5% CO_2 for 1 hour, and gently rocked every 15 min. After removal of the inocula, plates were overlaid with 1.2% agarose containing 4% FBS. Three days later, overlays were removed, and plaques were visualized using 0.1% crystal violet staining. Viral titers were quantified as PFU per milliliter of tissue. SARS-CoV-2 was inactivated by exposure to UV light for 1 hour using a wattage of 4016 $\mu W/cm^2$.

All cell lines were incubated at 37°C in 5% CO_2. Vero cells were grown in DMEM supplemented with 5% FBS, penicillin (100 IU/ml), and streptomycin (100 μg/ml). BHK21 cells were grown in DMEM containing 10% tryptose phosphate broth, 5% FBS, penicillin (100 IU/ml), and streptomycin (100 μg/ml).

Immunofluorescence and immunoblotting

Immunofluorescent localization of SARS-CoV-2-S protein expression was performed in MDBK cells in 24-well plates that were infected

with CVXGA1 or PIV5 at a multiplicity of infection (MOI) of 1. At 2 days after infection, the cells were washed with PBS and then fixed in 2% formaldehyde. The cells were permeabilized in 0.1% PBS-saponin solution and incubated for 1 hour with anti–SARS-CoV-2 S (Sino Biological, catalog no.40150-R007) and anti–PIV5-V/P at 1:200 dilution, and then fluorescein isothiocyanate–labeled goat anti-rabbit (KPL, catalog no. 02-15-16) and Cy3-labeled goat anti-mouse (KPL, catalog no. 072-01-18-06) secondary antibodies were added to the cells with 4′,6-diamidino-2-phenylindole (DAPI; 2 drops/ml; NucBlue Live Cell Stain ReadyProbes reagent, Life Technologies Corporation, Eugene, OR, USA). The cells were incubated for 30 min and were examined and photographed using a Nikon Eclipse Ti confocal fluorescence microscope.

Immunoblotting was performed on Vero cells that were infected in 12-well plates with PIV5 or CVXGA1 at an MOI of 1. At 24 hours post-infection (hpi), Laemmli sample buffer (Bio-Rad, catalog no. 1610737) with 5% β-mercaptoethanol was used to lyse cells. The lysates were separated on an SDS–polyacrylamide gel electrophoresis (SDS-PAGE) gel and immunoblotted with an anti–SARS-CoV-2-S antibody (Sigma-Aldrich, catalog no. ZHU1076) and an anti–PIV5-V/P antibody.

Purification of S and RBD of S

The plasmid encoding the complementary DNA for prefusion-stabilized SARS-CoV-2 spike ectodomain (*24*) was synthesized (Twist Bioscience) and cloned into the pTwist cytomegalovirus Hygro vector. The plasmid encoding the monomeric spike RBD was obtained from BEI Resources (NR-52309). The plasmids were expanded by transformation into *Escherichia coli* DH5α cells with ampicillin (100 μg/ml; Thermo Fisher Scientific) used for selection. Plasmids were purified using the E.Z.N.A. plasmid maxi kit (Omega Bio-tek), according to the manufacturer's protocol. For each liter of transfection, 1 mg of plasmid DNA was mixed with 4 mg of 25,000–molecular weight polyethylenimine (PEI; Polysciences Inc.) in 66 ml of Opti-MEM cell culture medium (Gibco). After 30 min, the DNA-PEI mixture was added to human embryonic kidney 293F cells (1 million cells/ml) in FreeStyle 293 medium (Gibco). After 5 to 7 days, the cultures were centrifuged to pellet the cells, and the supernatants were filtered through a 0.45-μm sterile filter. Recombinant proteins were purified from the filtered culture supernatants using HisTrap Excel columns (GE Healthcare Life Sciences). Each column was stored in 20% ethanol and washed with 5 column volumes (CV) of wash buffer [20 mM tris (pH 7.5), 500 mM NaCl, and 20 mM imidazole] before loading samples onto the column. After sample application, columns were washed with 10 CV of wash buffer. Proteins were eluted from the column with 6 CV of elution buffer [20 mM tris (pH 7.5), 500 mM NaCl, and 250 mM imidazole]. Proteins were concentrated and buffer-exchanged into PBS using Amicon Ultra-15 centrifugal filter units with a 30-kDa cutoff (Millipore Sigma).

Enzyme-linked immunosorbent assay

To quantify the anti–SARS-CoV-2-S humoral response after prime and after boost, mouse serum was analyzed via enzyme-linked immunosorbent assay (ELISA). Immulon 2HB 96-well microtiter plates were coated with 100 μl of purified SARS-CoV-2-S at 1 μg/ml. The serum was serially diluted twofold and incubated on the plates for 2 hours. Horseradish peroxidase (HRP)–labeled goat anti-mouse IgG secondary antibody (SouthernBiotech, Birmingham, AL) was diluted 1:2500 and incubated on the wells for 1 hour. The plates were developed with KPL SureBlue Reserve TMB microwell peroxidase substrate (SeraCare Life Sciences Inc., Milford, MA), and OD_{450} (optical density at 450 nm) values were detected with a BioTek Epoch microplate spectrophotometer (BioTek, Winooski, VT). Antibody endpoints were calculated as $\log_{10}$ of the highest serum dilution at which the OD_{450} value was greater than 2 SD above the mean OD_{450} value of naïve serum.

To detect ferret IgG, medium-binding 96-well ELISA microplates (Greiner Bio-One, 655001) were coated with 20 μg of either the full-length SARS-CoV-2 full spike protein or SARS-CoV-2 RBD (*27*) in sterile 1× PBS(Corning, 21-040-CV) overnight at 4°C. Plates were washed 3× with 300 μl of 0.05% PBS-T using an automated plate washer (BioTek 405 TS washer). All washes were performed using the same technique. Wells were blocked with 200 μl of blocking buffer [0.5% bovine serum albumin (BSA) + 3% nonfat dry milk in 0.05% PBS-T], incubated for 2 hours at room temperature, and then washed. Heat-inactivated serum was diluted in blocking buffer, and 100 μl was added to the appropriate wells and incubated for 2 hours at room temperature followed by a wash step. Goat anti-ferret IgG HRP-conjugated antibody (Bethyl Laboratories, A140-108P) diluted 1:5000 to 1:10,000 in blocking buffer was added at 100 μl per well and incubated for 1 hour at room temperature. Plates were washed and tapped dry to remove residual solutions. SIGMAFAST *o*-phenylenediamine dihydrochloride tablets (Sigma-Aldrich, P9187) for the detection of peroxidase activity were prepared in 20 ml of dH_20 and added at 100 μl per well. Following an 8-min development period, 50 μl of 1 N H_2SO_4 was added to stop the reaction. Immediately, plates were read at absorbance of 490 nm (BioTek, Cytation7 machine). Background signal was calculated from the average absorbance values obtained from capture protein–coated wells that received goat anti-ferret IgG-HRP antibody.

To detect ferret IgA, ELISA microplates were coated, blocked, and washed as for ferret IgG detection. Twofold serial dilutions of pooled, heat-inactivated, nasal wash sample (collected in PBS) were performed in blocking buffer, and 100 μl was added to the appropriate wells. Nasal wash dilutions were incubated for 2 hours at room temperature and washed, and goat anti-ferret IgA alkaline phosphatase (AP)–conjugated antibody (Rockland, 618-105-006) diluted 1:2000 in blocking buffer was added at 100 μl per well and incubated for 1 hour at room temperature. Plates were washed and tapped dry to remove residual solutions. Plates were developed and read as for ferret IgG ELISAs. Background signal was calculated from the average absorbance values obtained from capture protein–coated wells that received goat anti-ferret IgA AP antibody.

Immunization and infection of mice with SARS-CoV-2

Immunization

Six- to 8-week-old female mice (Envigo) or K18-hACE2 mice [B6.Cg.Tg(K18-hACE2)2Prlmn/J, Jackson Laboratory] were used in these studies. The mice were anesthetized by intraperitoneal injection of 250 μl of 2,2,2-tribromoethanol in *tert*-amyl alcohol (Avertin) and intranasally inoculated with 50 μl of PBS (or DMEM) or 10^4, 10^5, or 10^6 PFU of CVXGA1 or 10^6 PFU of PIV5 vector. Twenty-eight days after immunization, the mice were euthanized, serum was collected via cardiothoracic bleeds, and spleens were harvested. The mice were housed and immunized in enhanced BSL2 facilities in HEPA-filtered isolators. All experiments were performed in accordance with protocols approved by the IACUC at the University

of Georgia and at the University of Iowa. UV-inactivated SARS-CoV-2 (10^6 PFU) was 1:1 (v/v) mixed with alum adjuvant (Thermo Fisher Scientific, catalog no. 77161) in a volume of 200 μl and delivered to mice intramuscularly.

Infection of mice

Mice were lightly anesthetized with ketamine/xylazine and intranasally inoculated with the indicated amount of SARS-CoV-2 in a total volume of 50 μl of DMEM. Animal weight and health were monitored daily. All experiments with SARS-CoV-2 were performed in a BSL3 laboratory at the University of Iowa.

Immunization and infection of ferrets with SARS-CoV-2

Immunization of ferrets

Twelve 8- to 9-month-old male and female (700 to 2000 g) fitch ferrets were received from Triple F Farms and acclimated in the UGA animal facilities. Before arrival, ferrets underwent sterilization and scent gland removal. Following an acclimation period of at least 7 days, ferrets were anesthetized for subcutaneous placement of thermal transponders between the shoulder blades. Implantable Programmable Temperature Transponders (Bio Medic Data Systems, USA) were anchored securely to the tissue at the implantation site and allowed temperature readouts ranging from 32.2° to 43.3°C. Simultaneously, whole blood was collected for baseline serology, and fecal swab was performed for analysis of viral shedding.

Prechallenge procedures were performed at the University of Georgia Biosciences Animal Facility. Animals were housed in pairs with ad libitum access to food and water. Following vaccination, procedures, including nasal wash and blood collections, were performed on anesthetized animals using ketamine/xylazine (15 to 20 mg/kg/1 to 2 mg/kg of xylazine) delivered intramuscularly. Ferrets were monitored daily for clinical signs. Weights and temperatures were recorded, at minimum, during each procedure under sedation.

Viral challenge of ferrets

For SARS-CoV-2 challenge, animals were transferred to the University of Georgia Animal Health Research Center Animal BSL3 facility. Procedures performed after viral challenge were done under short-term isoflurane gas anesthesia.

Groups of six ferrets were vaccinated intranasally with 1×10^6 PFU of CVXGA1 in 1.0 ml of sterile PBS distributed as 500 μl per nostril. Following vaccination, animals were monitored daily for clinical signs, including nasal discharge, sneezing, diarrhea, lethargy, increased respiratory rate and effort (congestion), cyanosis, neurological changes, and altered responses to external stimuli. Body temperature was tracked using the implanted temperature probes. Nasal washes and fecal swabs were collected at 3, 7, 14, 21, and 28 dpi to assess vaccine shedding. Whole blood was obtained weekly following immunization. Peripheral blood mononuclear cells (PBMCs) were isolated and cryopreserved for future analysis. For infectious challenge with SARS-CoV-2, 1×10^6 PFU was delivered via the intranasal route. Again, physical observations, weights, and temperatures were measured daily. A subset of six animals were humanely euthanized and necropsied on day 4 after challenge, and the remaining animals ($n = 6$) were humanely euthanized on day 7 after challenge. All necropsies were performed under the guidance of a board-certified veterinary pathologist. Tissue samples (trachea and lung) were collected for pathology and viral load. Terminal blood collection was carried out for serum and PBMC isolation. For transmission study, at 2 dpc, two challenged ferrets were mixed with one naïve ferret.

Cohousing of ferrets

Two days after SARS-CoV-2 challenge, a naïve ferret was paired with one challenged ferret. The second challenged ferret was transferred to isolation caging until necropsy at 4 dpc. All experiments were approved by the IACUC of the University of Georgia.

Histology and immunohistochemistry

Mice were anesthetized and perfused transcardially with PBS. Lung tissues were harvested, fixed in 10% neutral-buffered formalin, dehydrated through a series of alcohol and xylene baths, paraffin-embedded, sectioned at ~4 μm, and stained with hematoxylin and eosin (H&E) stains. Tissues were examined by a boarded pathologist in a masked manner and following principles for reproducible tissue scores (*28*). Perivascular eosinophil infiltration was assessed as previously described (*9*). Briefly, perivascular regions with cellular infiltration were randomly selected ($n = 20$ per lung), and the number of eosinophils was enumerated and averaged for a final score for each lung. Perivascular lymphoid aggregates were ordinally scored: 0, absent; 1, few solitary cells; 2, moderate small to medium aggregates; or 3, robust aggregates forming circumferential perivascular cuffs with compression of adjacent parenchyma. Interstitial disease was ordinally scored using a modified H score: 0, absent; 1, minor scattered cells in septa; 2, moderate infiltrates in septa and extending into lumen; or 3, moderate to severe infiltrates in septa and lumen with associated consolidation/atelectasis and or edema. For each of the tiers, the percentage of lung affected was recorded. The final modified H score for each lung was calculated as follows: % affected × each tier score, summed, and then divided by 100 to yield a score between 0 and 3.

Immunohistochemistry was performed as previously described (*19*). Briefly, primary anti–SARS-CoV-2 N protein antibody (1:20,000 dilution × 60 min; 40143-R019, Sino Biological) was followed by rabbit EnVision (Dako) and diaminobenzidine (Dako) as chromogen with hematoxylin as counterstain. Ordinal scoring of immunostaining was performed in a distribution-based manner: 0, absent; 1, 0 to 25%; 2, 26 to 50%; 3, 51 to 75%; and 4, >75% of lung fields in tissue section.

SARS-CoV-2 S neutralization

Vesicular stomatitis virus (VSV) pseudotyped with SARS-CoV-2 (VSV-S) described previously was used for neutralization assay (*29*). VSV-S particles were titered by median tissure culture infectious dose in a 96-well plate in Vero cells to determine the optimal number of particles for neutralization. They were diluted in 2% FBS and 1% penicillin/streptomycin (P/S) in DMEM media. Titer was determined using Firefly luciferase–detected Bio-Glo Luciferase Assay System by Promega. A particle control was used on each plate that consisted of a 1:1 ratio of diluted particles and sterile PBS (no serum). A negative control was also used on each plate consisting of sterile PBS and 2% FBS and 1% P/S in DMEM media to account for background.

Serum was heat-inactivated at 56°C for 45 min before neutralization assay. It was then serially diluted in sterile PBS using 1:2 dilutions starting at 1:100 (ferrets) in a 96-well untreated plate containing no cells. A recovered human serum sample (+RHS) was used as a positive control in each assay and was serially diluted 1:2 starting at 1:100. Samples and controls were done in quadruplicate.

Diluted VSV-S particles (50 μl) were added to the 96-well plate containing 50 μl of diluted serum and incubated for 1 hour at

5% CO_2 at 37°C. After 1 hour, the media was aspirated from a white 96-well plate containing Vero cells at 90 to 100% confluency, and the particle-serum mixture (100 µl) was added to the cells. The plate was incubated at 5% CO_2 at 37°C for 18 to 24 hours. The next day, the media was aspirated, and 50 µl of Nano-Glo reagent was added to each well. Plates were agitated and then read immediately using the Renilla-Luciferase Protocol on a GloMax Luminometer by Promega.

For neutralization with SARS-CoV-2, serum samples were heat-inactivated at 56°C for 30 min before neutralization assay. They were then serially diluted in sterile DMEM and mixed with an equal volume of DMEM containing ~20 PFU of SARS-CoV-2. After incubation at 37°C for 1 hour, the aliquots were added into Vero E6 cells in 12-well plates and incubated at 37°C in 5% CO_2 for 1 hour. After the removal of inocula, plates were overlaid with 1.2% agarose containing 4% FBS. After further incubation at 37°C in 5% CO_2 for 2 days, overlays were removed, and plaques were visualized by staining with 0.1% crystal violet.

SARS-CoV-2 nasal shedding qPCR

RNA extraction and generation of a standard curve

For the SARS-CoV-2 RNA genome standard curve, 1.1×10^6 PFU/ml or 1.44×10^7 PFU/ml for ferret and feline standards, respectively, was inactivated by dilution 1:1 (v/v) with TRIzol Reagent (Thermo Fisher Scientific) according to inactivation protocols. RNA was extracted from 600 µl of the diluted virus using a Direct-zol RNA Miniprep Plus kit (Zymo Research) and eluted in 50 µl of DNA/RNA-free water according to protocol. RNA purity [absorbance at 260 nm (A_{260})/A_{280}] and concentration were assessed using a DeNovix DS-11 FX+ spectrophotometer/fluorometer (DeNovix). RNA was stored at −80°C. For the standard curve, RNA was diluted 10-fold, and 10 µl of each RNA dilution was used in a 40-µl qPCR reaction with 10 µl of TaqPath 1-Step RT-qPCR Master Mix (Thermo Fisher Scientific) and 3 µl of nCov N1 primer/probe from EUA CDC SARS-2 kit (Integrated DNA Technologies). For nasal wash samples, 500 µl of recovered nasal wash or rectal swab sample was inactivated by dilution 1:1 with 2× DNA/RNA Shield (Zymo Research) and stored at −20°C until extraction. RNA was extracted from 600 µl of the diluted sample using a Quick RNA Viral Kit (Zymo Research) and eluted in 15 µl of DNA/RNA-free water according to protocol. RNA purity (A_{260}/A_{280}) and concentration were assessed using a DeNovix DS-11 FX+ spectrophotometer/fluorometer. RNA was stored at −80°C. All qPCR reactions were analyzed using an Agilent Mx3000P.

Ferret nasal wash qPCR

qPCR was performed using TaqPath 1-Step RT-qPCR Master Mix (Thermo Fisher Scientific) on an Agilent Mx3000P qPCR System. Each nasal wash reaction consisted of 10 µl of TaqPath, 3 µl of primer/probe mix, 17 µl of water, and 10 µl of sample diluted to 2 ng for a final reaction volume of 40 µl per well. The nCoV N gene–specific primers (forward, 5′-GACCCCAAAATCAGCGAAAT-3′; reverse, 5′-TCTGGTTACTGCCAGTTGAATCTG-3′) and probe [5′-(FAM)ACCCCGCATTACGTTTGGTGGACC(BHQ1)-3′] were purchased from Integrated DNA Technologies as part of the RUO CDC SARS-2 kit. The thermal profile consisted of 1 cycle for 2 min at 25°C, 1 cycle for 15 min at 50°C, 1 cycle for 2 min at 95°C, and 50 cycles of 3 s at 95°C then 30 s at 55°C. qPCR runs for each plate included RNA standards (10-fold dilutions, 10 µl per reaction, in duplicate), no template control, no polymerase control, and a sample spiked with viral RNA for a positive control. PFU-per-milliliter concentration of each sample was determined using the original PFU-per-milliliter concentration of the viral stock used for the RNA standard curve. The ratio of RNA used in the qPCR reaction was calculated by dividing 2 ng by the total RNA concentration per sample. The PFU-per-milliliter output from the standard curve was multiplied by the ratio of RNA used in the reaction, and the total PFU-per-milliliter content of the sample was determined through back calculation using the dilution and extraction volumes described. Samples with Ct values greater than 37 were considered PCR negative. For each qPCR plate, 1 PFU/PCR reaction Ct value was established from the standard curve and set as $y = 0$, the limit of detection was set at the standard curve concentration at the Ct value of 37, and the challenge dose was included for reference. All samples between 1 PFU/reaction and the limit of detection are considered PCR positive but having noninfectious genomic material.

Ferret tissue qPCR

Tissue samples were inactivated with 1× DNA/RNA Shield at a ratio of 1 ml of Shield per 100 mg of tissue. The tissue was bead-homogenized (TissueLyser II, Qiagen) at a frequency of 30 for 1.5 min, and the homogenate was stored at −20°C until extraction. The extraction process was the same as for nasal washes. Ferret tissues were assayed using the above protocol with the following exceptions. Each reaction consisted of 6.66 µl of TaqPath, 2 µl of primer/probe mix, 20.34 µl of water, and 1 µl of sample for a final reaction volume of 30 µl per well. Hypoxanthine-guanine phosphoribosyltransferase (HPRT) was used as a housekeeping gene to ensure the presence of tissue RNA in the absence of viral RNA. The HPRT gene–specific primers (forward, 5′-CACTGGGAAAACAATGCA-GA-3′; reverse, 5′-ACAAAGTCAGGTTTATAGCCAACA-3′) were synthesized by Integrated DNA Technologies. The gene-specific TaqMan MGB probe (5′-NED-TGCTGGTGAAgAGGAC-CCCTCG-MGBNFQ-3′) was synthesized by Applied Biosystems. HPRT fluorescence was read using the HEX absorption and emission spectra. PFU-per-milliliter concentration of each sample was determined using the original PFU-per-milliliter concentration of the viral stock used for the RNA standard curve. The total PFU-per-milliliter content of the sample was determined through back calculation using the dilution and extraction volumes described to PFU per milliliter of homogenate. Samples with Ct values greater than 37 were considered PCR negative. For each qPCR plate, 1 PFU/ml Ct value was established from the standard curve and set as $y = 0$, and the limit of detection was set at the standard curve concentration at the Ct value of 37. All samples between 1 PFU/ml and the limit of detection are considered PCR positive but having noninfectious genomic material. For graphing purpose, CT values less than 37, but more than the 1 PFU/reaction cutoff, were assigned a genome copy per milliliter value of 0.5.

Focus-forming unit assay

Ferret nasal wash samples were assayed for infectious SARS-CoV-2 by focus-forming units (FFU) on Vero E6 cells. Briefly, 96-well cell culture plates were seeded at 3.2×10^5 cells per well and incubated overnight. Confluent monolayers were incubated with 10-fold serial dilutions of inoculum in culture media of DMEM containing 2% FBS and 1× antibiotic/antimycotic media. For growth media from culture plates, 50 µl of inoculum was incubated for 1 hour at 37°C, 5% CO_2 with humidity. Overlay media, 0.8% methylcellulose in culture media, was applied at 150 µl per well, and the plates were returned to 37°C, 5% CO_2 with humidity for 20 to 24 hours. For

colorimetric development of FFU, methylcellulose overlay was decanted, and plates were washed three times with 1× PBS. Fixative solution (80% methanol and 20% acetone) was added at 100 µl and allowed to incubate for a minimum of 10 min at room temperature before submersion in fixative solution and removal from BSL3 facilities. Primary antibody (HRP-conjugated 1C02; 1.4 µg/ml) was diluted to 1:1000 in blocking buffer (0.1% Tween 20, 5% nonfat dry milk, and 5% BSA) at 75 µl per well and incubated at room temperature for 45 min. Next, primary solution was decanted, and plates were washed twice with 0.1% PBS-T. An additional wash step was completed with dH_2O, with 75 µl per well of TMB development solution added, and incubated at room temperature for 1 hour. A final dH_2O wash step was completed, plates were air-dried, and images were obtained with the BioTek Cytation7 machine for manual FFU quantification.

SUPPLEMENTARY MATERIALS

Supplementary material for this article is available at http://advances.sciencemag.org/cgi/content/full/7/27/eabi5246/DC1

REFERENCES AND NOTES

1. R. Wölfel, V. M. Corman, W. Guggemos, M. Seilmaier, S. Zange, M. A. Müller, D. Niemeyer, T. C. Jones, P. Vollmar, C. Rothe, M. Hoelscher, T. Bleicker, S. Brünink, J. Schneider, R. Ehmann, K. Zwirglmaier, C. Drosten, C. Wendtner, Virological assessment of hospitalized patients with COVID-2019. *Nature* **581**, 465–469 (2020).
2. N. Li, X. Wang, T. Lv, Prolonged SARS-CoV-2 RNA shedding: Not a rare phenomenon. *J. Med. Virol.* **92**, 2286–2287 (2020).
3. Q. Gao, L. Bao, H. Mao, L. Wang, K. Xu, M. Yang, Y. Li, L. Zhu, N. Wang, Z. Lv, H. Gao, X. Ge, B. Kan, Y. Hu, J. Liu, F. Cai, D. Jiang, Y. Yin, C. Qin, J. Li, X. Gong, X. Lou, W. Shi, D. Wu, H. Zhang, L. Zhu, W. Deng, Y. Li, J. Lu, C. Li, X. Wang, W. Yin, Y. Zhang, C. Qin, Development of an inactivated vaccine candidate for SARS-CoV-2. *Science* **369**, 77–81 (2020).
4. H. Wang, Y. Zhang, B. Huang, W. Deng, Y. Quan, W. Wang, W. Xu, Y. Zhao, N. Li, J. Zhang, H. Liang, L. Bao, Y. Xu, L. Ding, W. Zhou, H. Gao, J. Liu, P. Niu, L. Zhao, W. Zhen, H. Fu, S. Yu, Z. Zhang, G. Xu, C. Li, Z. Lou, M. Xu, C. Qin, G. Wu, G. F. Gao, W. Tan, X. Yang, Development of an inactivated vaccine candidate, BBIBP-CorV, with potent protection against SARS-CoV-2. *Cell* **182**, 713–721.e9 (2020).
5. N. B. Mercado, R. Zahn, F. Wegmann, C. Loos, A. Chandrashekar, J. Yu, J. Liu, L. Peter, K. M. Mahan, L. H. Tostanoski, X. He, D. R. Martinez, L. Rutten, R. Bos, D. van Manen, J. Vellinga, J. Custers, J. P. Langedijk, T. Kwaks, M. J. G. Bakkers, D. Zuijdgeest, S. K. Rosendahl Huber, C. Atyeo, S. Fischinger, J. S. Burke, J. Feldman, B. M. Hauser, T. M. Caradonna, E. A. Bondzie, G. Dagotto, M. S. Gebre, E. Hoffman, C. Jacob-Dolan, M. Kirilova, Z. Li, Z. Lin, S. H. Mahrokhian, L. F. Maxfield, F. Nampanya, R. Nityanandam, J. P. Nkolola, S. Patel, J. D. Ventura, K. Verrington, H. Wan, L. Pessaint, A. Van Ry, K. Blade, A. Strasbaugh, M. Cabus, R. Brown, A. Cook, S. Zouantchangadou, E. Teow, H. Andersen, M. G. Lewis, Y. Cai, B. Chen, A. G. Schmidt, R. K. Reeves, R. S. Baric, D. A. Lauffenburger, G. Alter, P. Stoffels, M. Mammen, J. Van Hoof, H. Schuitemaker, D. H. Barouch, Single-shot Ad26 vaccine protects against SARS-CoV-2 in rhesus macaques. *Nature* **586**, 583–588 (2020).
6. K. S. Corbett, B. Flynn, K. E. Foulds, J. R. Francica, S. Boyoglu-Barnum, A. P. Werner, B. Flach, S. O'Connel, K. W. Bock, M. Minai, B. M. Nagata, H. Andersen, D. R. Martinez, A. T. Noe, N. Douek, M. M. Donaldson, N. N. Nji, G. S. Alvarado, D. K. Edwards, D. R. Flebbe, E. Lamb, N. A. Doria-Rose, B. C. Lin, M. K. Louder, S. O'Dell, S. D. Schmidt, E. Phung, L. A. Chang, C. Yap, J.-P. M. Todd, L. Pessaint, A. Van Ry, S. Browne, J. Greenhouse, T. Putman-Taylor, A. Strasbaugh, T.-A. Campbell, A. Cook, A. Dodson, K. Steingrebe, W. Shi, Y. Zhang, O. M. Abiona, L. Wang, A. Pegu, E. S. Yang, K. Leung, T. Zhou, I.-T. Teng, A. Widge, I. Gordon, L. Novik, R. A. Gillespie, R. J. Loomis, J. I. Moliva, G. Stewart-Jones, S. Himansu, W.-P. Kong, M. C. Nason, K. M. Morabito, T. J. Ruckwardt, J. E. Ledgerwood, M. R. Gaudinski, P. D. Kwong, J. R. Mascola, A. Carfi, M. G. Lewis, R. S. Baric, A. M. Dermott, I. N. Moore, N. J. Sullivan, M. Roederer, R. A. Seder, B. S. Graham, Evaluation of the mRNA-1273 vaccine against SARS-CoV-2 in nonhuman primates. *N. Engl. J. Med.* **383**, 1544–1555 (2020).
7. N. van Doremalen, T. Lambe, A. Spencer, S. Belij-Rammerstorfer, J. N. Purushotham, J. R. Port, V. Avanzato, T. Bushmaker, A. Flaxman, M. Ulaszewska, F. Feldmann, E. R. Allen, H. Sharpe, J. Schulz, M. Holbrook, A. Okumura, K. Meade-White, L. Pérez-Pérez, C. Bissett, C. Gilbride, B. N. Williamson, R. Rosenke, D. Long, A. Ishwarbhai, R. Kailath, L. Rose, S. Morris, C. Powers, J. Lovaglio, P. W. Hanley, D. Scott, G. Saturday, E. de Wit, S. C. Gilbert, V. J. Munster, ChAdOx1 nCoV-19 vaccination prevents SARS-CoV-2 pneumonia in rhesus macaques. *bioRxiv* 2020.05.13.093195 , (2020).
8. Z. Chen, M. Zhou, X. Gao, G. Zhang, G. Ren, C. W. Gnanadurai, Z. F. Fu, B. He, A novel rabies vaccine based on a recombinant parainfluenza virus 5 expressing rabies virus glycoprotein. *J. Virol.* **87**, 2986–2993 (2013).
9. K. Li, Z. Li, C. Wohlford-Lenane, D. K. Meyerholz, R. Channappanavar, D. An, S. Perlman, P. B. McCray Jr., B. He, Single-dose, intranasal immunization with recombinant parainfluenza virus 5 expressing Middle East respiratory syndrome coronavirus (MERS-CoV) spike protein protects mice from fatal MERS-CoV infection. *MBio* **11**, e00554-20 (2020).
10. A. J. Mooney, Z. Li, J. D. Gabbard, B. He, S. M. Tompkins, Recombinant parainfluenza virus 5 vaccine encoding the influenza virus hemagglutinin protects against H5N1 highly pathogenic avian influenza virus infection following intranasal or intramuscular vaccination of BALB/c mice. *J. Virol.* **87**, 363–371 (2013).
11. S. I. Phan, Z. Chen, P. Xu, Z. Li, X. Gao, S. L. Foster, M. N. Teng, R. A. Tripp, K. Sakamoto, B. He, A respiratory syncytial virus (RSV) vaccine based on parainfluenza virus 5 (PIV5). *Vaccine* **32**, 3050–3057 (2014).
12. S. I. Phan, J. R. Zengel, H. Wei, Z. Li, D. Wang, B. He, Parainfluenza virus 5 expressing wild-type or prefusion respiratory syncytial virus (RSV) fusion protein protects mice and cotton rats from RSV challenge. *J. Virol.* **91**, e00560-17 (2017).
13. H. J. Cornwell, I. A. McCandlish, H. Thompson, H. M. Laird, N. G. Wright, Isolation of parainfluenza virus SV5 from dogs with respiratory disease. *Vet. Rec.* **98**, 301–302 (1976).
14. E. J. Kontor, R. J. Wegrzyn, R. A. Goodnow, Canine infectious tracheobronchitis: Effects of an intranasal live canine parainfluenza-Bordetella bronchiseptica vaccine on viral shedding and clinical tracheobronchitis (kennel cough). *Am. J. Vet. Res.* **42**, 1694–1698 (1981).
15. Z. Chen, P. Xu, G. W. Salyards, S. B. Harvey, B. Rada, Z. F. Fu, B. He, Evaluating a parainfluenza virus 5-based vaccine in a host with pre-existing immunity against parainfluenza virus 5. *PLOS ONE* **7**, e50144 (2012).
16. D. Wang, S. Phan, D. J. Di Stefano, M. P. Citron, C. L. Callahan, L. Indrawati, S. A. Dubey, G. J. Heidecker, D. Govindarajan, X. Liang, B. He, A. S. Espeseth, A single-dose recombinant parainfluenza virus 5-vectored vaccine expressing respiratory syncytial virus (RSV) F or G protein protected cotton rats and african green monkeys from RSV challenge. *J. Virol.* **91**, e00066-17 (2017).
17. P. B. McCray Jr., L. Pewe, C. Wohlford-Lenane, M. Hickey, L. Manzel, L. Shi, J. Netland, H. P. Jia, C. Halabi, C. D. Sigmund, D. K. Meyerholz, P. Kirby, D. C. Look, S. Perlman, Lethal infection of K18-*hACE2* mice infected with severe acute respiratory syndrome coronavirus. *J. Virol.* **81**, 813–821 (2007).
18. R.-D. Jiang, M.-Q. Liu, Y. Chen, C. Shan, Y.-W. Zhou, X.-R. Shen, Q. Li, L. Zhang, Y. Zhu, H.-R. Si, Q. Wang, J. Min, X. Wang, W. Zhang, B. Li, H.-J. Zhang, R. S. Baric, P. Zhou, X.-L. Yang, Z.-L. Shi, Pathogenesis of SARS-CoV-2 in transgenic mice expressing human angiotensin-converting enzyme 2. *Cell* **182**, 50–58.e8 (2020).
19. J. Zheng, L.-Y. R. Wong, K. Li, A. K. Verma, M. E. Ortiz, C. Wohlford-Lenane, M. R. Leidinger, C. M. Knudson, D. K. Meyerholz, P. B. McCray Jr., S. Perlman, COVID-19 treatments and pathogenesis including anosmia in K18-hACE2 mice. *Nature* **589**, 603–607 (2021).
20. Y.-I. Kim, S.-G. Kim, S.-M. Kim, E.-H. Kim, S.-J. Park, K.-M. Yu, J.-H. Chang, E. J. Kim, S. Lee, M. A. B. Casel, J. Um, M.-S. Song, H. W. Jeong, V. D. Lai, Y. Kim, B. S. Chin, J.-S. Park, K.-H. Chung, S.-S. Foo, H. Poo, I.-P. Mo, O.-J. Lee, R. J. Webby, J. U. Jung, Y. K. Choi, Infection and rapid transmission of SARS-CoV-2 in ferrets. *Cell Host Microbe* **27**, 704–709. e2 (2020).
21. J. Shi, Z. Wen, G. Zhong, H. Yang, C. Wang, B. Huang, R. Liu, X. He, L. Shuai, Z. Sun, Y. Zhao, P. Liu, L. Liang, P. Cui, J. Wang, X. Zhang, Y. Guan, W. Tan, G. Wu, H. Chen, Z. Bu, Susceptibility of ferrets, cats, dogs, and other domesticated animals to SARS-coronavirus 2. *Science* **368**, 1016–1020 (2020).
22. M. Richard, A. Kok, D. de Meulder, T. M. Bestebroer, M. M. Lamers, N. M. A. Okba, M. F. van Vlissingen, B. Rockx, B. L. Haagmans, M. P. G. Koopmans, R. A. M. Fouchier, S. Herfst, SARS-CoV-2 is transmitted via contact and via the air between ferrets. *Nat. Commun.* **11**, 3496 (2020).
23. E. S. Winkler, A. L. Bailey, N. M. Kafai, S. Nair, B. T. McCune, J. Yu, J. M. Fox, R. E. Chen, J. T. Earnest, S. P. Keeler, J. H. Ritter, L.-I. Kang, S. Dort, A. Robichaud, R. Head, M. J. Holtzman, M. S. Diamond, SARS-CoV-2 infection of human ACE2-transgenic mice causes severe lung inflammation and impaired function. *Nat. Immunol.* **21**, 1327–1335 (2020).
24. D. Wrapp, N. Wang, K. S. Corbett, J. A. Goldsmith, C.-L. Hsieh, O. Abiona, B. S. Graham, J. S. McLellan, Cryo-EM structure of the 2019-nCoV spike in the prefusion conformation. *Science* **367**, 1260–1263 (2020).
25. A. J. Mooney, J. D. Gabbard, Z. Li, D. A. Dlugolenski, S. K. Johnson, R. A. Tripp, B. He, S. M. Tompkins, Vaccination with recombinant parainfluenza virus 5 expressing neuraminidase protects against homologous and heterologous influenza virus challenge. *J. Virol.* **91**, e01579-17 (2017).

26. Z. Li, A. J. Mooney, J. D. Gabbard, X. Gao, P. Xu, R. J. Place, R. J. Hogan, S. M. Tompkins, B. He, Recombinant parainfluenza virus 5 expressing hemagglutinin of influenza A virus H5N1 protected mice against lethal highly pathogenic avian influenza virus H5N1 challenge. *J. Virol.* **87**, 354–362 (2013).
27. F. Amanat, D. Stadlbauer, S. Strohmeier, T. H. O. Nguyen, V. Chromikova, M. M. Mahon, K. Jiang, G. A. Arunkumar, D. Jurczyszak, J. Polanco, M. Bermudez-Gonzalez, G. Kleiner, T. Aydillo, L. Miorin, D. S. Fierer, L. A. Lugo, E. M. Kojic, J. Stoever, S. T. H. Liu, C. Cunningham-Rundles, P. L. Felgner, T. Moran, A. García-Sastre, D. Caplivski, A. C. Cheng, K. Kedzierska, O. Vapalahti, J. M. Hepojoki, V. Simon, F. Krammer, A serological assay to detect SARS-CoV-2 seroconversion in humans. *Nat. Med.* **26**, 1033–1036 (2020).
28. D. K. Meyerholz, A. P. Beck, Principles and approaches for reproducible scoring of tissue stains in research. *Lab. Invest.* **98**, 844–855 (2018).
29. K. E. Havranek, A. R. Jimenez, M. D. Acciani, M. F. L. Mendoza, J. M. R. Ballista, D. A. Diaz, M. A. Brindley, SARS-CoV-2 spike alterations enhance pseudoparticle titers and replication-competent VSV-SARS-CoV-2 Virus. *Viruses* **12**, 1465 (2020).

Acknowledgments: We thank C. Wohlford-Lenane, K. Kulhankova, S. Ray, and A. Lorton for technical assistance. We thank J. Barber for assistance with the fluorescent confocal microscopy. We thank the animal resources and veterinary staff for support of the animal studies. Plasmids for expression of SARS-CoV-2 spike and RBD proteins were provided by F. Krammer (Icahn School of Medicine at Mount Sinai, produced under contract NIAID CEIRS contract HHSN272201400008C). Plasmids for expression of the 1C02 anti–SARS-CoV-2 spike protein monoclonal antibody were provided by A. Ellebedy (Washington University School of Medicine, St. Louis). SARS-related coronavirus 2, isolate USA-WA1/2020 (NR-52281), was deposited by the Centers for Disease Control and Prevention and obtained through BEI Resources, NIAID, NIH. **Funding:** This work is supported by CyanVac LLC. P.B.M. is supported by the Roy J. Carver Charitable Trust. B.H. is supported by Fred C. Davison Distinguished University Professor in Veterinary Medicine. **Author contributions:** Conceptualization and writing—original draft: P.B.M., S.M.T., and B.H.; formal analysis: D.A., M.C.H.D., A.C.B., K.B., G.L., S.K.J., K.L., D.K.R., D.K.M., P.B.M., S.M.T., and B.H.; investigation: D.A., M.C.H.D., A.C.B., K.B., G.L., Y.L., S.K.J., K.L. D.K.R., J.H., E.F.G., S.K.J., I.P., C.A.J., J.M., M.B., K.S., D.K.M., P.B.M., S.M.T., and B.H.; visualization: A.C.B., D.K.R., E.F.G., and D.K.M.; resources: J.M., M.B., D.K.M., P.B.M., S.M.T., and B.H.; writing—review and editing: A.C.B., D.K.R., E.F.G., K.S., P.B.M., S.M.T., and B.H.; supervision: P.B.M., S.M.T., and B.H.; project administration: P.B.M., S.M.T., and B.H.; funding acquisition: P.B.M., S.M.T., and B.H. **Competing interests:** B.H. is an inventor of patent "PIV5-based vaccines," which is owned by the University of Georgia Research Foundation. B.H. is an inventor of a provisional patent application on CVXGA1 that has been filed by the University of Georgia Research Foundation (2021-008, filed on 1 August 2021). B.H. is a founder and owner of CyanVac LLC, which supported this work. M.C.H.D., K.B., and A.C.B. consulted for CyanVac LLC and also have stock options in CyanVac LLC–affiliated entity. All other authors declare that they have no competing interests. **Data and materials availability:** All data needed to evaluate the conclusions in the paper are present in the paper and/or the Supplementary Materials. SARS-CoV-2 can be provided by S.M.T. pending scientific review and a completed material transfer agreement. Requests for the SARS-CoV-2 should be submitted to the University of Georgia Research Foundation. CVXGA1 can be provided by B.H. pending scientific review and a completed material transfer agreement. Requests for the CVXGA1 should be submitted to the University of Georgia Research Foundation. Additional data related to this paper may be requested from the authors.

Submitted 15 March 2021
Accepted 21 May 2021
Published 2 July 2021
10.1126/sciadv.abi5246

Citation: D. An, K. Li, D. K. Rowe, M. C. H. Diaz, E. F. Griffin, A. C. Beavis, S. K. Johnson, I. Padykula, C. A. Jones, K. Briggs, G. Li, Y. Lin, J. Huang, J. Mousa, M. Brindley, K. Sakamoto, D. K. Meyerholz, P. B. McCray Jr., S. M. Tompkins, B. He, Protection of K18-hACE2 mice and ferrets against SARS-CoV-2 challenge by a single-dose mucosal immunization with a parainfluenza virus 5–based COVID-19 vaccine. *Sci. Adv.* **7**, eabi5246 (2021).

Science Advances

Protection of K18-hACE2 mice and ferrets against SARS-CoV-2 challenge by a single-dose mucosal immunization with a parainfluenza virus 5–based COVID-19 vaccine

Dong An, Kun Li, Dawne K. Rowe, Maria Cristina Huertas Diaz, Emily F. Griffin, Ashley C. Beavis, Scott K. Johnson, Ian Padykula, Cheryl A. Jones, Kelsey Briggs, Geng Li, Yuan Lin, Jiachen Huang, Jarrod Mousa, Melinda Brindley, Kaori Sakamoto, David K. Meyerholz, Paul B. McCray, Jr., S. Mark Tompkins and Biao He

Sci Adv **7** (27), eabi5246.
DOI: 10.1126/sciadv.abi5246